Petroleum Science 18 (2021) 1729–1738

Contents lists available at ScienceDirect

Petroleum Science

journal homepage: www.keaipublishing.com/en/journals/petroleum-science

Original Paper

A novel predictive model of drag coefficient and settling velocity of drill cuttings in non-Newtonian drilling fluids

Tie Yan [a], Jing-Yu Qu [a, *], Xiao-Feng Sun [a], Wei Li [a], Ye Chen [b], Qiao-Bo Hu [a]

[a] College of Petroleum Engineering, Northeast Petroleum University, Daqing, 163318, Heilongjiang, People's Republic of China
[b] Sinopec Shale Gas Research Institute of Petro China Southwest Oil and Gas Field, Chengdu, 610051, Sichuan, People's Republic of China

ARTICLE INFO

Article history:
Received 4 February 2021
Accepted 28 June 2021
Available online 3 September 2021

Edited by Yan-Hua Sun

Keywords:
Drag coefficient
Settling velocity
Non-Newtonian fluid
Drill cuttings
Hole cleaning

ABSTRACT

In oil and gas well drilling operations, it is of great significance to accurately predict the drag coefficient and settling velocity of drill cuttings in non-Newtonian drilling fluids. In this paper, the free-falling of 172 groups of spheres and 522 groups of irregular-shaped sand particles in Newtonian/non-Newtonian fluids were investigated experimentally. It was found that the drag coefficient calculated based on Newtonian correlations can result in a significant error when the particle settles in the non-Newtonian fluid. Therefore, predictive models of drag coefficient were established respectively for different types of fluids. The validity of the proposed drag coefficient model of spheres was verified by comparing it with the previous works. On this basis, the drag coefficient model of irregular-shaped sand particles was established by introducing a shape factor. The models do not use the shape factor that requires detailed three-dimensional shape and size information. Instead, two-dimensional geometric information (circularity) is obtained via image analysis techniques. The present new models predict the settling velocity of sand particles in the power-law fluid and Herschel–Bulkley fluid accurately with a mean relative error of 5.03% and 6.74%, respectively, which verifies the accuracy of the model.

1. Introduction

In oil and gas well drilling operations, drilling operations often must be temporarily stopped due to operations such as replacing a dull bit or making a connection. The circulation of drilling fluid in the annulus must be terminated during the temporary stop (Agwu et al., 2018). Drill cuttings begin to settle and deposit at the bottom of the hole, resulting in a hole cleaning problem. Inadequate hole cleaning can lead to some drilling problems, such as the high drag and torque, stuck pipe, circulation loss, and well instability, which increase operational costs (Guan et al., 2016; Sayindla et al., 2017). Accurate calculation of the cuttings settling velocity allows the cuttings deposition behavior to be effectively predicted and the hole-cleaning performance to be effectively evaluated. Settling velocity is sometimes required as an input for optimization and design calculations (Okesanya et al., 2020). Settling velocity can also be used to estimate the formation depth from which the cuttings are generated. Important information such as lithology, porosity, permeability, and pore pressure can be obtained based on cuttings analysis (Baldino et al., 2015).

The fluid drag force acting on a single free-falling particle is proportional to the square of its settling velocity. After a short period of initial acceleration, the force acting on the particles reaches equilibrium. The particles eventually settle at a constant velocity, the so-called settling velocity (also called the "terminal" or "final" velocity). In a multiphase flow, the particle-fluid drag force F_d can be expressed as:

$$F_d = \frac{\pi}{8}\rho_l C_d d_{eq}^2 v_s^2 \tag{1}$$

where ρ_l is the fluid density; d_{eq} is the equivalent diameter, $d_{eq} = \sqrt[3]{6m_p/\pi\rho_s}$; m_p is the mass of particle, when the particle is spherical, d_{eq} is equal to diameter; ρ_s is the particle density; C_d is the drag coefficient; v_s is the terminal settling velocity.

The terminal settling velocity is the constant velocity of free settling particles, which is achieved when gravity force (F_g), buoyancy force (F_b), and fluid drag force (F_d) balance. The drag coefficient is defined as the ratio of the viscous drag force to the kinetic energy acting on the falling particle. This is a parameter that primarily describes the settling behavior of the particle. The drag coefficient can be calculated by the nature of the fluid and particles and the settling velocity (Stokes, 1851):

* Corresponding author.
E-mail address: qujingyu0411@163.com (J.-Y. Qu).

https://doi.org/10.1016/j.petsci.2021.09.003

$$C_d = \frac{4}{3}\frac{g d_{eq}}{v_s^2}\frac{\rho_s - \rho_l}{\rho_l} \quad (2)$$

where g is the acceleration of gravity. For a smooth sphere, the drag coefficient is a function of the particle Reynolds number Re_s, that is $C_d = f(Re_s)$. The particle Reynolds number is another main parameter describing the settling behavior of the particle. It is defined as the ratio of the inertial force to the viscous force experienced by the particle. In a Newtonian fluid, it is defined as follows (Clift et al., 1978):

$$Re_s = \frac{\rho_f v_s d_{eq}}{\mu} \quad (3)$$

where μ is the Newtonian fluid viscosity.

In 1851, Stokes proposed his analytical solution of the drag force exerted by the fluid on a sphere under very slow or creeping flow conditions ($Re_s < 0.1$); this is the well-known "Stokes' law" ($C_d = 24/Re_s$) (Stokes, 1851). Many scholars have investigated the free-falling of smooth spheres across a broad range of particle Reynolds numbers in the following 170 years. The relationship between C_d and Re_s is usually linked as an empirical correlation due to the difficulty of obtaining an analytical solution. A considerable number of correlations already have high prediction accuracy (e.g., Schiller and Naumann, 1933; Morsi and Alexander, 1972; Clift et al., 1978; Levenspiel and Haider, 1989; Brown and Lawler, 2003; Cheng, 2009; Barati et al., 2014). These research works can be comprehensively summarized and well-reviewed in several published review papers (Agwu et al., 2018; Goossens, 2019) and communication articles (Ramírez, 2017; Barati and Neyshabouri, 2018).

The correlations mentioned above were developed for Newtonian fluids. However, nearly all drilling fluids are non-Newtonian, which exhibit complicated rheological characteristics such as shear-thinning or yield stress behavior. Particles settle differently in non-Newtonian fluids than the Newtonian fluids as well. The definitions of particle Reynolds number or apparent viscosity need to be modified to ensure that the settling results coincide with the standard Newtonian drag curve. This approach ensures uniformity for various Newtonian and non-Newtonian fluids and allows for convenient settling velocity predictions (Okesanya and Kuru, 2019). The modified Re_s for a particle falling in power-law fluid and Herschel–Bulkley fluid are as follows (Acharya et al., 1976; Machač et al., 1995). For the power-law fluids:

$$Re_s = \frac{\rho_f v_s^{2-n} d_{eq}^n}{K} \quad (4)$$

And for the Herschel–Bulkley fluids:

$$Re_s = \frac{\rho_f v_s^{2-n} d_{eq}^n}{K + \tau_0\left(\frac{d_{eq}}{v_s}\right)^n} \quad (5)$$

where τ_0 is the yield stress, K is the consistency coefficient, and n is the flow index. These parameters can be used to define the rheology of a power-law fluid or Herschel–Bulkley fluid; The rheological models are defined as follows. For the power-law fluid:

$$\tau = K\dot{\gamma}^n \quad (6)$$

and for the Herschel–Bulkley fluid:

$$\tau = \tau_0 + K\dot{\gamma}^n \quad (7)$$

where τ is the shear stress and $\dot{\gamma}$ is the shear rate.

It is not only that the drilling fluid is mostly non-Newtonian fluid, but also the cuttings encountered in actual drilling are irregular in shape. Unlike spherical particles, the drag coefficient is a function of both particle Reynolds number and shape for an irregular-shaped particle. Cuttings with different shapes have different stress states in the non-Newtonian drilling fluid leading to variant settling velocities, and the settlement behavior is more complex. Many researchers have described particle shape irregularity (e.g., sphericity, circularity, roundness, and Corey shape factor) and established drag coefficient correlations as a function of the shape factor (Dioguardi and Mele, 2015; Wang et al., 2018; Xu et al., 2019; Sun et al., 2020). Sphericity is the most widely used, which is defined as the ratio between the surface area of the equivalent sphere and that of the actual particle. However, compared to non-spherical particles with regular shapes, it is difficult to measure the surface area of rough or fragile particles like drill cuttings, and also difficult to practice in the field; indeed, it is one of the most challenging parameters to be determined (Dioguardi and Mele, 2015). Breakey et al. (2018) found that the predictions using 2D side-view geometric data with an accuracy close to that achieved by other correlations that require 3D geometric data of particle surface area and volume. And detailed 3D knowledge of cuttings' geometry can only be obtained through careful laboratory measurements. Even in a laboratory setting, these measurements are not trivial (and frequently impossible to obtain) for non-spherical cuttings particles.

A given prediction model is not likely to be popular or even applicable in the petroleum engineering field if it relies on complex measurement methods to describe irregular-shaped cuttings particles. Dioguardi and Mele (2015) found that the circularity is more suitable when the secondary motions (such as rotations, oscillation tumbling, etc.) of falling particles are not taken into account in the analysis. With the increase of Reynolds number, the instability of the separated shear layer will increase, and the phenomenon of secondary motion will appear. Circularity is a 2D parameter that is sensible to the irregularity of the contour of particles. It is defined as the ratio of the maximum projection perimeter and the perimeter of the circle equivalent to the maximum projection area. Fang (1992) pointed out that the cuttings settling is swinging when $Re_s > 100$, whereas the settling is stable when $Re_s < 100$. We believe that it is achievable to introduce the circularity c to establish the drag coefficient correlations for irregular-shaped cuttings in non-Newtonian fluid as $Re_s < 100$. That is to say, the shape factor description method that requires detailed 3D shape parameters may not be used, and the drag coefficient and settling velocity of the drill cuttings can be predicted only through the 2D shape information.

In this study, we experimentally tested the settling velocity of spherical particles and irregular-shaped sand particles in Newtonian and non-Newtonian fluids. We used image analysis technology to identify the circularity of the irregular-shaped sand particle and introduced it into the drag coefficient prediction model. The proposed models show better prediction performance for the settling velocity of irregular-shaped sand particles in non-Newtonian fluids. Such information is of great importance for predicting the settling velocity of irregular-shaped drill cuttings in non-Newtonian drilling fluids in the petroleum industry, and for perfecting the cuttings transport model of irregular-shaped cuttings.

2. Experimental methods

2.1. Experimental setups and procedures

A photo of our settling experiment setup is shown in Fig. 1. The experiment was carried out in a transparent plexiglass cylinder with an inner diameter of 100 mm and a height of 1500 mm. The image acquisition area was set at least 300 mm away from the bottom of the cylinder. A high-speed camera (Revealer 2F04C) was used to capture the settling process. The camera was connected directly to a computer for data storage. The recording speed was 200 f/s. A high-frequency lamp illumination source (Jinbei EF-200 LED) and a white background were used to enhance the clarity of particles in the image. The images registered were explored and analyzed by image-treatment software.

The experiment was initiated by gently dropping a test particle into the tube as close to the center as possible via a tweezer. The data from any experiments in which the particle settling trajectory deviated substantially from the central vertical line of the cylinder were discarded. To minimize any uncertainty, each experiment of the sphere was repeated in three replications, and only the data with a maximum relative error of less than 5% was reserved for fitting the drag coefficient correlation. However, each sand particle has unique shape and size parameters. We chose to increase the number of settling experiments to minimize the influence of abnormal experimental data on the fitting results.

2.2. Test materials and fluid rheology

The test spherical particles were fabricated from steel, zirconia, and glass to eliminate the influence of single material particles on the measurement results. The white quartz sand was selected for the irregular-shaped particle settling experiment. The particle-to-cylinder diameter ratio was kept small to reduce the influence of the wall effect on the data. The properties of the test particles are shown in Table 1.

Different concentrations of glycerol, carboxymethyl cellulose (CMC), and Carbopol aqueous solutions were selected as the test fluids with different rheological models. This design also gave the experiment data a broad range of particle Reynolds numbers. After mixing the aqueous glycerol solution, the mixture fluid was sealed for at least 12 h. Similarly, CMC powder, Carbopol powder, and tap water were mixed and sealed to hydrate for at least 24 h. Before the experiment, the test fluid was transferred into the cylinder and left for enough time for the air bubbles to escape. The samples were collected to measure their rheological parameters at the test temperature with an advanced rotational rheometer (Anton Paar MCR 92) between 1 and 1000 1/s shear rates. The fluid parameters were fitted according to the corresponding rheological model. A total of 18 types of fluids with different rheological parameters were used in the settling experiment. Their rheological parameters are listed in Table 2.

Fig. 1. Experimental setup layout to measure the settling velocity.

Table 1
Properties of test particles.

Type of material	Particle size d_{eq}, mm	Density ρ_s, kg/m^3
Steel	1, 2, 3, 4, 5	7930
Zirconia	1.0, 1.3, 1.5	6080
Glass	1, 2, 3, 4, 5	2500
Quartz sand particle	2.1–5.7	2650

2.3. Measurement of particle shape factor

The sand particles were placed in a small LED studio, and the maximum projection plane was exposed to a camera (Nikon 1 J5) above. Each image was taken with a 5568 × 3712 pixel resolution. Using an image digital analysis program ImageJ (National Institutes of Health, USA), to determine the circularity of particles. The original digital image with an RGB color format captured by the camera was first converted into an eighth-order grayscale image. A grey-level-based threshold method was used to identify the particle edge. The threshold value was set based on the difference between the image background and the particle. The circularity of the target particles on the image was measured using the "Analyze Particles" function of ImageJ. The definition of circularity proposed in the ImageJ user guide is (Ferreira and Rasband, 2012):

$$c = 4\pi \times \frac{A_P}{P_p^2} \tag{8}$$

c is the particle circularity; A_P is the area of maximum projection; P_P is the perimeter of maximum projection.

Similar to sphericity, for a spherical particle, $c = 1$, whereas for a projection of any other shape, $c < 1$. An example of the image conversion for irregular-shaped sand particles is shown in Fig. 2.

The distribution of circularity and equivalent diameter parameters of all 522 groups of sand particles used in the experiment are shown in Fig. 3. The equivalent diameter of the sand particles used in the experiment is 2.1–5.7 mm, with a median of 3.6 mm. And the circularity is 0.35–0.87, with a median of 0.75. The circularity of most sand particles is concentrated between 0.7 and 0.8.

3. Results and discussion

We first carried out experimental measurements on the settling velocity of spheres to develop a correlation between C_d calculated by Eq. (2) and Re_s calculated using Eqs. (3)–(5). The experimental data of 172 groups of spheres settling velocities were analyzed, then the C_d–Re_s relationship was plotted on a logarithmic scale (Fig. 4). When the particle Reynolds number is low, the distribution of the drag coefficient in different types of fluids conforms to the predicted trend of Stokes' law. It is observed that the drag coefficient curve of Newtonian fluid is in close agreement with Stokes' law, but contains a substantial error in the power-law fluid and Herschel–Bulkley fluid. For example, in the case of Re_s<0.1, the mean relative error (MRE) between the experimental result in Newtonian fluid and the prediction result of Stokes' law is only 2.32%. The MRE of that in the power-law fluid and Herschel–Bulkley fluid is 30.16% and 16.02%, respectively. The fluid

Table 2
Rheological properties of test fluids.

Test fluids	Temperature, °C	Density, kg/m^3	Rheological parameters		
			τ_0, Pa	K, Pa s^n	n
100 wt% glycerine	24.9	1260	0	0.8646	1
95 wt% glycerine	24.3	1250	0	0.3682	1
90 wt% glycerine	24.2	1230	0	0.1646	1
80 wt% glycerine	25.2	1210	0	0.044	1
50 wt% glycerine	25.2	1116	0	0.005267	1
2 wt% CMC	18.8	1005	0	4.7703	0.4781
1.75 wt% CMC	18.5	1004	0	2.921	0.5103
1.5 wt% CMC	20.1	1003	0	1.8028	0.5469
1.25 wt% CMC	18.6	1002.5	0	1.0256	0.5845
1 wt% CMC	20.0	1002	0	0.4927	0.637
0.5 wt% CMC	18.3	1001	0	0.0805	0.7697
0.25 wt% CMC	16.7	1000	0	0.0189	0.8886
0.125 wt% Carbopol	18.6	1000	2.5108	0.53235	0.63178
0.12 wt% Carbopol	18.5	1000	1.7841	0.42042	0.65337
0.115 wt% Carbopol	17.6	1000	1.3999	0.36572	0.66535
0.11 wt% Carbopol	17.3	1000	0.8463	0.27032	0.68951
0.105 wt% Carbopol	16.9	1000	0.5051	0.20109	0.71679
0.10 wt% Carbopol	19.8	1000	0.2152	0.136	0.7677

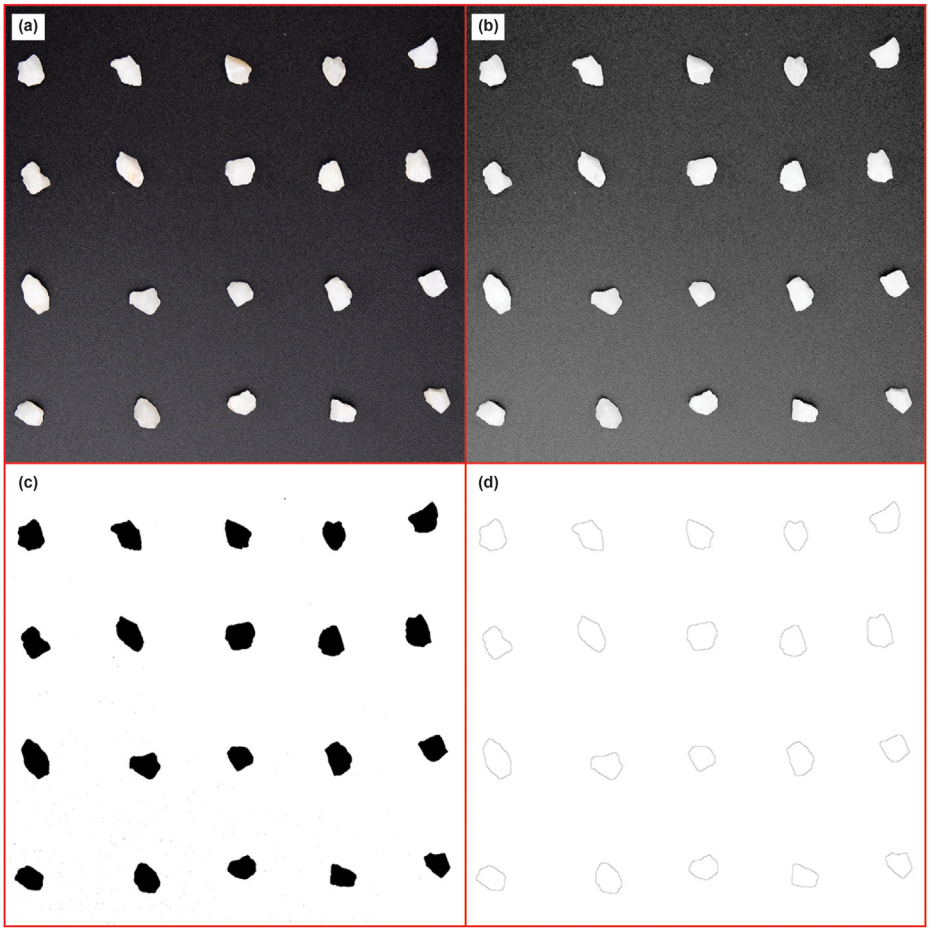

Fig. 2. An example of image conversion of irregular-shaped sand particles. (**a**) Original RGB image. (**b**) Converted into an eighth-order grayscale image. (**c**) Thresholding of eight-bit image. (**d**) Drawing outlines.

behavior index and yield stress are important rheological parameters that affect fluid–particle interactions. In this case, the drag coefficient of a sphere in non-Newtonian fluid calculated based on Newtonian correlations can result in a significant error.

We expect to establish a unified C_d–Re_s relationship based on the experimental data obtained to predict the sphere drag coefficient in the Newtonian fluid, power-law fluid, and Herschel–Bulkley fluid. And model switching between fluids with different rheological properties can be avoided. A unified form of prediction correlation can facilitate the construction of subsequent cuttings transport model. The drag coefficient and settling velocity can be predicted by modifying the relevant coefficients in the

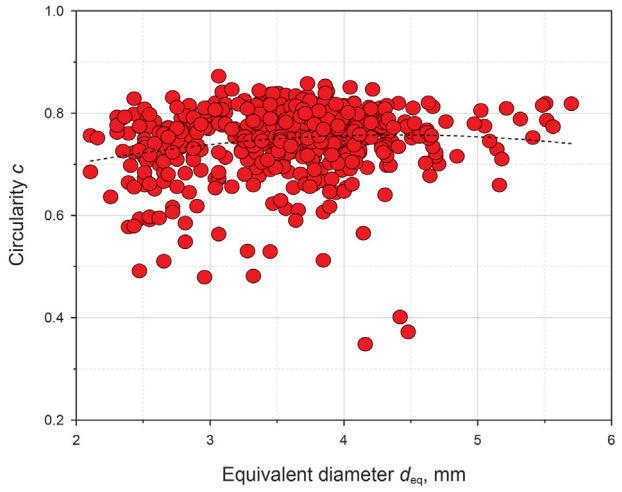

Fig. 3. Distribution of circularity and equivalent diameter.

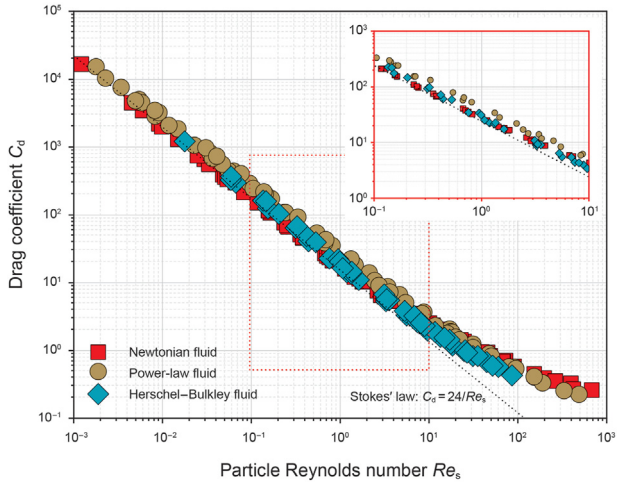

Fig. 4. Presentation of all spheres data and C_d–Re_s relationships.

model for fluids with different rheological properties. And the C_d–Re_s correlations can be extended and applied to irregular-shaped sand particles. We reviewed several expressions of drag coefficients (e.g., Schiller and Naumann, 1933; Levenspiel and Haider, 1989; Cheng, 2009), each having a different accuracy and range of applicability. We found that the five-parameter formula (Eq. (9)) modified by Levenspiel and Haider (1989) has the best goodness-of-fit:

$$C_d = \frac{24}{Re_s}\left(1 + ARe_s^B\right) + \frac{C}{1 + D/Re_s^E} \tag{9}$$

where A, B, C, D, and E are the correlation constants. The first term on the right of Eq. (9) represents the decreasing trend of drag coefficient under laminar flow conditions. The second term represents the reduced decreasing trend under turbulent conditions. The drag coefficient can be predicted by adding a complex turbulent Newton's term to the extended Stokes's law. This inference is supported by the scientific fundamental that the total drag is the sum of laminar and turbulent components in any flow regime (Goossens, 2019).

Regression analysis was performed on the 172 groups settling data to obtain drag coefficient relations of spheres in the Newtonian fluid, power-law fluid, and Herschel–Bulkley fluid. For Newtonian fluids:

$$C_d = \frac{24}{Re_s}\left(1 + 0.174Re_s^{0.632}\right) + \frac{0.292}{1 + \frac{1765.61}{Re_s}} \quad \text{for } 0.001 < Re_s < 680 \tag{10}$$

for power-law fluids:

$$C_d = \frac{24}{Re_s}\left(1 + 0.741Re_s^{0.185}\right) + \frac{0.269}{1 + \frac{55.13}{Re_s^{1.63}}} \quad \text{for } 0.001 < Re_s < 490 \tag{11}$$

and for Herschel–Bulkley fluids:

$$C_d = \frac{24}{Re_s}\left(1 + 0.282Re_s^{0.229}\right) - \frac{167.28}{1 - \frac{33000}{Re_s}} \quad \text{for } 0.018 < Re_s < 86 \tag{12}$$

To evaluate the drag coefficient prediction performance of the proposed model, we compared Eqs. (10)–(12) against previous representative correlations (Table 3) for the spheres falling in Newton/non-Newtonian fluids. Three statistical parameters were used to evaluate the presented model further, and the evaluation results are listed in Table 4. MRE, maximum MRE, and root mean square of logarithmic error (RMSLE) were used to quantify the difference between the experimental and predicted values. MRE and RMSLE were calculated as follows:

$$\text{MRE} = \frac{1}{N}\sum_{i=1}^{N}\frac{\left|C_{d,cal,i} - C_{d,mea,i}\right|}{C_{d,mea,i}} \times 100\% \tag{13}$$

$$\text{RMSLE} = \sqrt{\frac{1}{N}\sum_{i=1}^{N}\left(\ln C_{d,cal,i} - \ln C_{d,mea,i}\right)^2} \tag{14}$$

where N is the total number, $C_{d,cal}$ represents predicted drag coefficient, and $C_{d,mea}$ represents measured drag coefficient.

As shown in Table 4, the predicted drag coefficients in the Newtonian fluid by Eqs. (15)–(17) are close to the experimental results; the average error is less than 4%. This further confirms the reliability of the experimental measurements. For power-law fluid and Herschel–Bulkley fluid, we found that the experimental results are close to the predicted values of Eqs. (18)–(20), with an average error of about 15.6%. We believe that one reason for the error is attributed to the different data points selected in fitting the rheological parameters of the non-Newtonian fluid. The proposed model (Eqs. (10)–(12)) has a certain degree of reduction in the three quantitative indicators and has a higher prediction accuracy for the experimental results compared to the other models we assessed. The MRE of the predicted value in power-law fluid and Herschel–Bulkley fluid are 6.38% and 6.59%, respectively, indicating the accuracy of proposed correlations.

The above drag coefficient prediction model (Eqs. (10)–(12)) was applied to spheres. Then, we introduced circularity c to improve the drag coefficient prediction accuracy of irregular-shaped sand particles. At any given Reynolds number, the drag of an irregular particle is greater than that of a sphere (Dioguardi et al., 2018). In irregular particles, surface irregularities lead to increased drag force and greater flow separation, thus reducing the settling velocity compared to that of spherical particles (Shahi and Kuru, 2015). We made this observation in our experiments as well

Table 3
Examples of C_d–Re_s correlations.

Reference	C_d–Re_s empirical correlations	Eq.
Brown and Lawler (2003) (Newtonian-)	$C_d = \frac{24}{Re_s}\left(1+0.15Re_s^{0.681}\right)+\frac{0.407}{1+8710/Re_s}$ for $Re_s<2\times10^5$	(15)
Cheng (2009) (Newtonian-)	$C_d = \frac{24}{Re_s}(1+0.27Re_s)^{0.43}+0.47\left[1-\exp(-0.04Re_s^{0.38})\right]$ for $Re_s<2\times10^5$	(16)
Levenspiel and Haider (1989) (Newtonian-)	$C_d = \frac{24}{Re_s}\left(1+0.186Re_s^{0.6459}\right)+\frac{0.4251}{1+6880.95/Re_s}$ for $Re_s<2.6\times10^5$	(17)
Khan and Richadson (1987) (Power-law- &Herschel–Bulkley-)	$C_d = \left(2.25Re_s^{-0.31}+0.36Re_s^{0.06}\right)^{3.45}$ for $1<Re_s<1000$	(18)
Machač et al. (1995) (Power-law- &Herschel–Bulkley-)	$C_d = \frac{24}{Re_s}X(n)$ for $Re_s<1$ $C_d = \frac{24}{Re_s}X(n)+\frac{10.5n-3.5}{Re_s^{0.32n+0.13}}$ for $1<Re_s<1000$ $X(n) = 3^{(3n-3)/2}\frac{33n^5-64n^4-11n^3+97n^2+16n}{4n^2(n+1)(n+2)(2n+1)}$	(19)
Okesanya et al. (2020) (Herschel–Bulkley-)	$C_d = \frac{24}{Re_s}(1+0.12Re_s)^{0.35}+0.398\left[1-\exp(-0.01Re_s^{0.9282})\right]$	(20)

Table 4
Prediction results of different models.

Reynolds number range	Investigator	Prediction error		
		MRE	RMSLE	Max. error
Newtonian fluids:				
$0.001<Re_s<680$	Brown and Lawler (2003)	3.47%	0.045	14.77%
	Cheng (2009)	3.72%	0.048	13.70%
	Levenspiel and Haider (1989)	3.29%	0.043	15.77%
	This study (Eq. (10))	2.69%	0.033	10.59%
Power-law fluids:				
$0.001<Re_s<490$	Khan and Richadson (1987)	17.29%	0.23	37.21%
	Machač et al. (2009)	12.19%	0.14	30.23%
	This study (Eq. (11))	6.38%	0.08	18.93%
Herschel–Bulkley fluids:				
$0.018<Re_s<86$	Khan and Richadson (1987)	17.09%	0.18	41.6%
	Machač et al. (1995)	19.56%	0.25	32.86%
	Okesanya et al. (2020)	11.90%	0.15	25.02%
	This study (Eq. (12))	6.59%	0.08	17.31%

(Fig. 5). The ratio of irregular-shaped particle drag coefficient C_d to that of a sphere $C_{d,sph}$, under the same conditions, should be slightly greater than 1. And the ratio is more significant at high Reynolds numbers because of the influence of shape.

We analyzed the difference between the sand particles' experimental C_d and the spheres' prediction values $C_{d,sph}$ under the same parameters. It is convenient to use circularity $f(c)$ as a function of the natural logarithm of $C_d/C_{d,sph}$. Thus, the relationship form between particle shape factor c and $C_d/C_{d,sph}$ is determined as follows:

$$C_d = C_{d,sph}\exp[f(c)] \tag{21}$$

When $c = 1$, in extreme cases, the drag coefficient of sand particles should be equal to that of a sphere. That is, when $c = 1$, $f(c) = 0$. In order to ensure that $C_d/C_{d,sph} = 1$ in the case of spherical particles, we determined the relationship of $f(c)$ by Eq. (22), based on our 522 sets of experimental data.

$$f(c) = \alpha Re_s^{\beta}(1-c)^{\lambda} \tag{22}$$

where α, β, and λ are the correlation constants, obtained by applying nonlinear fitting. The expressions are as follows. For Newtonian fluids:

$$C_d = C_{d,sph}\exp\left[0.25Re_s^{0.24}(1-c)^{0.49}\right] \quad \text{for } 0.02<Re_s<99 \tag{23}$$

for power-law fluids:

$$C_d = C_{d,sph}\exp\left[0.14Re_s^{0.41}(1-c)^{0.29}\right] \quad \text{for } 0.003<Re_s<86 \tag{24}$$

and for Herschel–Bulkley fluids:

$$C_d = C_{d,sph}\exp\left[0.6Re_s^{0.43}(1-c)^{1.23}\right] \quad \text{for } 0.13<Re_s<15 \tag{25}$$

The predicted drag coefficient $C_{d,sph}\exp f(c)$ calculated by the proposed models (Eqs. (23)–(25)) were compared against the experimental values calculated using Eq. (2), as shown in Fig. 6. And the evaluation results of the proposed model are listed in Table 5. The MRE of the predicted drag coefficient is 4.22%.

Now we established unified C_d–Re_s correlations for irregular-shaped sand particles in Newtonian/non-Newtonian fluids. The settling velocity can be calculated by using the Newton iterative method. And a trial-and-error method (as shown in Fig. 7) is required if settling velocity is calculated using the above C_d–Re_s relationship.

According to the proposed drag coefficient models of spheres (Eqs. (10)–(12)), C_d and Re_s of the falling sphere were calculated through trial and error procedures, as shown in Fig. 8. As seen in Fig. 8(a) that the predicted drag coefficient of the sphere in a

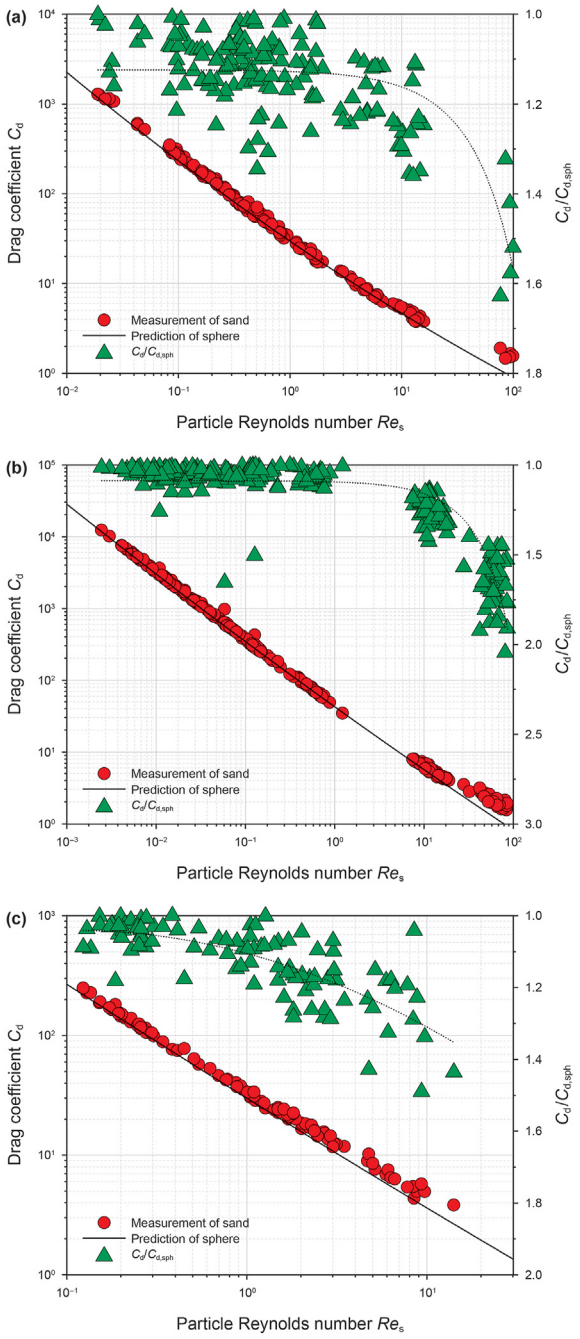

Fig. 5. Presentation of all sand particles data and C_d–Re_s relationships. (**a**) Newtonian fluid. (**b**) Power-law fluid. (**c**) Herschel–Bulkley fluid.

Newtonian fluid, power-law fluid, and Herschel–Bulkley fluid is in good agreement with the experimental value, with an MRE of 14.43%. At the same time, as seen in Fig. 8(b) that the predicted settling velocity has an MRE of 6.77% compared to the experimental data. The proposed model can better predict C_d and v_s of the sphere in fluids with different rheological properties.

Next, according to the proposed models (Eqs. (23)–(25)), the drag coefficients of irregular-shaped sand particles in fluids with different rheological properties were calculated as above and compared with the experimental data (Fig. 9). The predicted drag coefficient of sand particles in a Newtonian fluid, power-law fluid, and Herschel–Bulkley fluid have MRE of 8.04%, 8.99%, and 13.61%, respectively. In Newtonian fluids, especially when the particle

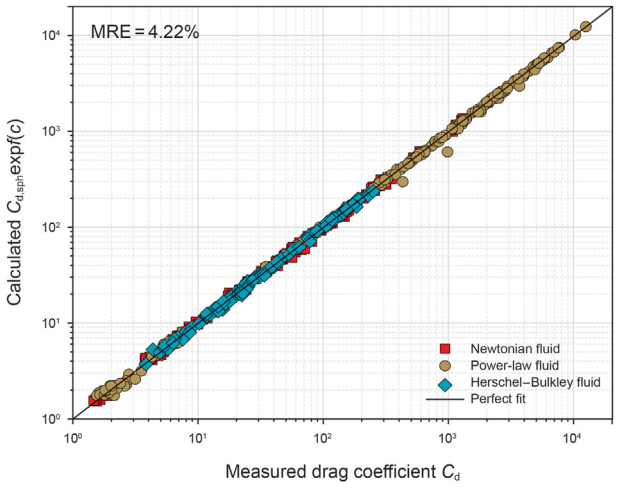

Fig. 6. Comparison of measured drag coefficient C_d and calculated $C_{d,sph}\exp f(c)$.

Table 5
Prediction error of proposed model for irregular-shaped particles.

Fluid type	Reynolds number range	Prediction error		
		MRE	RMSLE	Max error
Newtonian fluids	$0.02<Re_s<99$	4.59%	0.059	17.08%
Power-law fluids	$0.003<Re_s<86$	4.10%	0.065	37.74%
Herschel–Bulkley fluids	$0.13<Re_s<15$	3.98%	0.051	22.10%

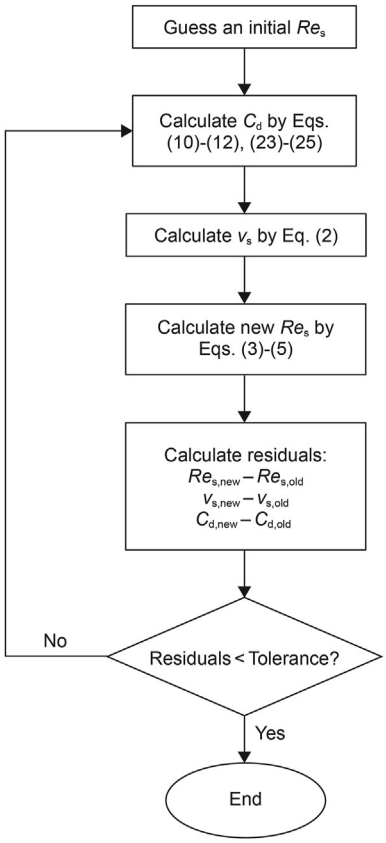

Fig. 7. Flow chart of the iterative procedure.

Reynolds number is large, a large MRE occurs. One reason is that the irregular-shaped sand particles do not fall steadily. The

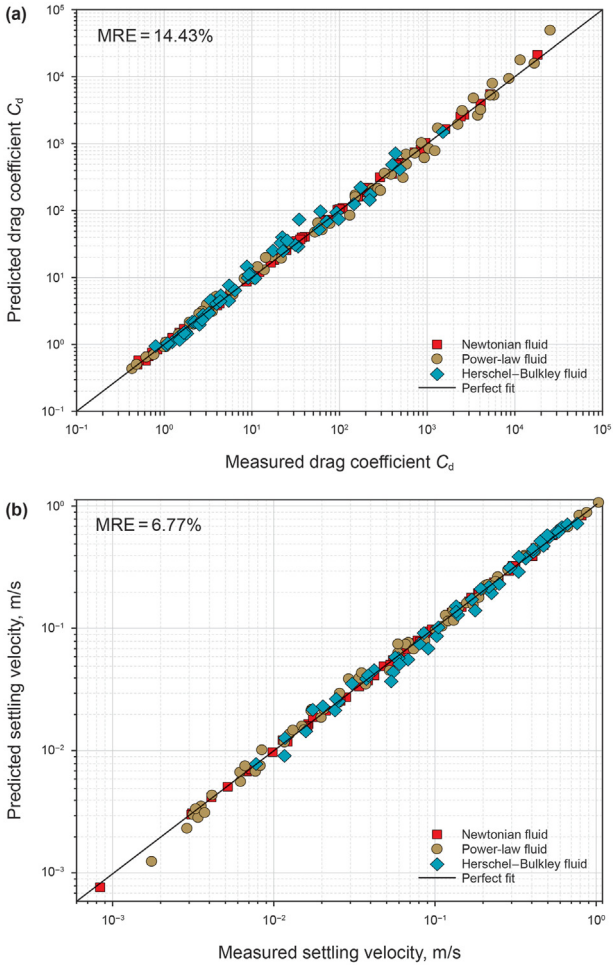

Fig. 8. Comparison of predicted results and experimental results. (**a**) Drag coefficient. (**b**) Settling velocity.

secondary motions (such as rotations, oscillation tumbling, etc.) affecting the fall trajectory of the irregular particles are easy to found in a Newtonian fluid with low viscosity, which leads to significant error relative to power-law fluid and Herschel–Bulkley fluid. The reason is that the Reynolds number of particles will be larger when the particles settle in the Newtonian fluid with low viscosity. With the increase of Reynolds number, the instability of the separated shear layer will increase, and the phenomenon of secondary motion will appear. The frequency of these secondary movements seems to lessen or fade if the sedimentation process occurs in non-Newtonian fluids in this paper.

Fig. 10 compares the predicted settling velocity and experimental settling velocity of sand particles in a Newtonian fluid, power-law fluid, and Herschel–Bulkley fluid. The MRE of the settling velocity in a Newtonian fluid, power-law fluid, and Herschel–Bulkley fluid is 4.04%, 5.03%, and 6.74%, respectively. Although there is a certain degree of dispersion with our model, the data is well distributed in a straight line. The proposed model appears to reasonably predict the settling velocity of the experimentally measured irregular-shaped particles.

4. Conclusions

In this study, two groups of new models were proposed to predict drag coefficient and settling velocity, based on 172 groups of spheres and 522 groups of irregular-shaped sand particles settling

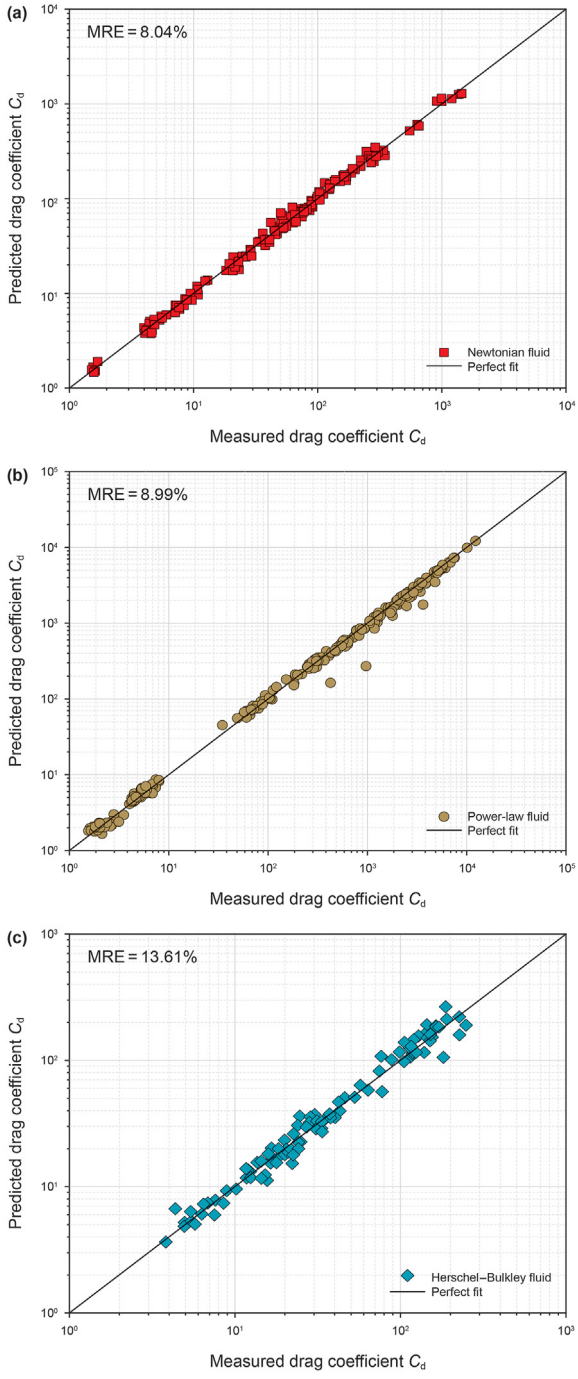

Fig. 9. Comparison of predicted and experimental drag coefficient. (**a**) Newtonian fluid. (**b**) Power-law fluid. (**c**) Herschel–Bulkley fluid.

in a Newtonian fluid, power-law fluid, and Heschel–Bulkley fluid. One group of models were proposed to predict the drag coefficients of sphere settling in Newtonian/non-Newtonian fluids by modifying the correlations proposed by Levenspiel and Haider (1989). Another group of models for irregular-shaped sand particles settling in Newtonian/non-Newtonian fluids were proposed based on the prediction models for spheres; the shape factor (circularity *c*) is introduced to describe the 2D geometric parameters through image analysis technology. The settling velocity can be calculated by using the Newton iterative method. The predicted data were in close agreement with the experimental data. This work may provide a valuable reference for people interested in cuttings settling

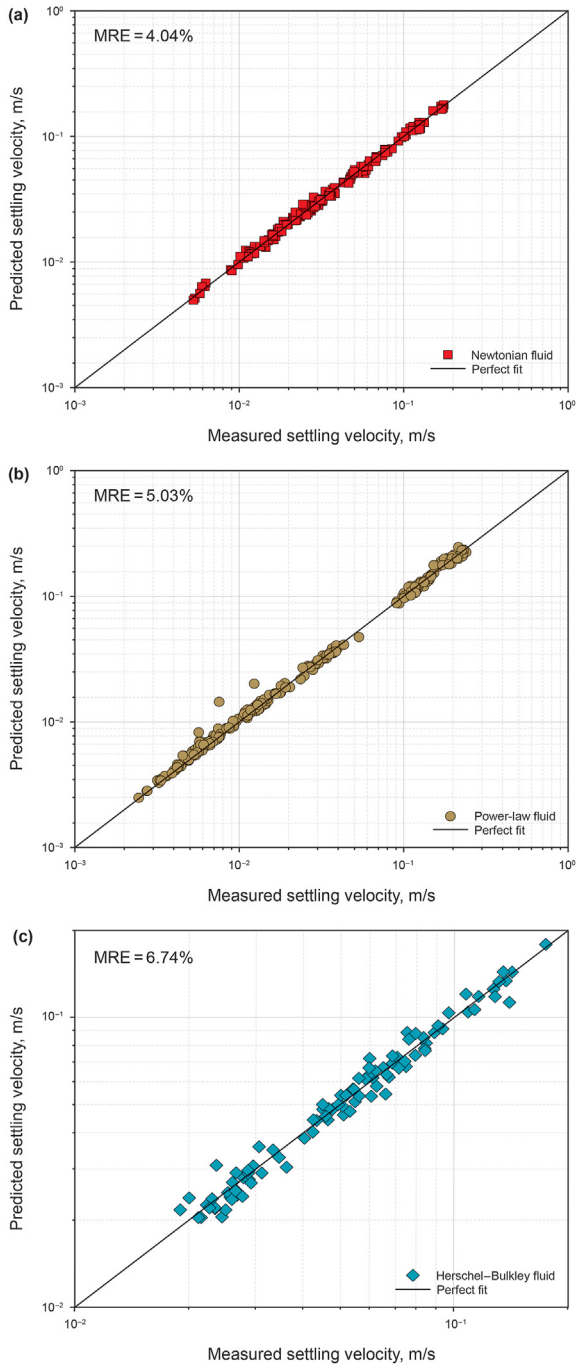

Fig. 10. Comparison of predicted and experimental settling velocity. (**a**) Newtonian fluid. (**b**) Power-law fluid. (**c**) Herschel–Bulkley fluid.

velocity, cuttings transport, and hole cleaning in drilling engineering scenarios.

Declaration of competing interest

The authors declare no conflict of interest.

Acknowledgements

This work was financially supported by the National Natural Science Foundation of China (Grant no. 51674087, 51974090) and the National Science and Technology Major Project of the Ministry of Science and Technology of China (grant number 2017ZX05009-003).

References

Acharya, A., Mashelkar, R.A., Ulbrecht, J., 1976. Flow of inelastic and viscoelastic fluids past a sphere - Part II: anomalous separation in the viscoelastic fluid flow. Rheol. Acta 15, 471–478. https://doi.org/10.1007/BF01530349.

Agwu, O.E., Akpabio, J.U., Alabi, S.B., Dosunmu, A., 2018. Settling velocity of drill cuttings in drilling fluids: a review of experimental, numerical simulations and artificial intelligence studies. Powder Technol. 339, 728–746. https://doi.org/10.1016/j.powtec.2018.08.064.

Baldino, S., Osgouei, R.E., Ozbayoglu, E., Miska, S., Takach, N., May, R., Clapper, D., 2015. Cuttings settling and slip velocity evaluation in synthetic drilling fluids. Offshore Mediterr. Conf. Exhib. OMC 1–15, 2015.

Barati, R., Neyshabouri, S.A.A.S., 2018. Comment on "Summary of frictional drag coefficient relationships for spheres: evolving solution strategies applied to an old problem". Chem. Eng. Sci. 181, 90–91. https://doi.org/10.1016/j.ces.2018.02.013.

Barati, R., Neyshabouri, S.A.A.S., Ahmadi, G., 2014. Development of empirical models with high accuracy for estimation of drag coefficient of flow around a smooth sphere: an evolutionary approach. Powder Technol. 257, 11–19. https://doi.org/10.1016/j.powtec.2014.02.045.

Breakey, D.E.S., Vaezi, G.F., Masliyah, J.H., Sanders, R.S., 2018. Side-view-only determination of drag coefficient and settling velocity for non-spherical particles. Powder Technol. 339, 182–191. https://doi.org/10.1016/j.powtec.2018.07.056.

Brown, P.P., Lawler, D.F., 2003. Sphere drag and settling velocity revisited. J. Environ. Eng. 129, 222–231. https://doi.org/10.1061/(asce)0733-9372(2003)129:3(222).

Cheng, N.S., 2009. Comparison of formulas for drag coefficient and settling velocity of spherical particles. Powder Technol. 189, 395–398. https://doi.org/10.1016/j.powtec.2008.07.006.

Clift, R., Grace, J.R., Weber, M.E., 1978. Bubbles, Drops, and Particles. Academic Press, New York.

Dioguardi, F., Mele, D., 2015. A new shape dependent drag correlation formula for non-spherical rough particles. Experiments and results. Powder Technol. 277, 222–230. https://doi.org/10.1016/j.powtec.2015.02.062.

Dioguardi, F., Mele, D., Dellino, P., 2018. A new one-equation model of fluid drag for irregularly shaped particles valid over a wide range of Reynolds number. J. Geophys. Res. Solid Earth. 123, 144–156. https://doi.org/10.1002/2017JB014926.

Fang, G., 1992. An experimental study of free settling of cuttings in Newtonian and non-Newtonian drillings fluids: drag coefficient and settling velocity. Soc. Pet. Eng. 1–13.

Ferreira, T., Rasband, W., 2012. ImageJ User Guide, ImageJ/Fiji.

Goossens, W.R.A., 2019. Review of the empirical correlations for the drag coefficient of rigid spheres. Powder Technol. 352, 350–359. https://doi.org/10.1016/j.powtec.2019.04.075.

Guan, Z.C., Liu, Y.M., Liu, Y.W., Xu, Y.Q., 2016. Hole cleaning optimization of horizontal wells with the multi-dimensional ant colony algorithm. J. Nat. Gas Sci. Eng. 28, 347–355. https://doi.org/10.1016/j.jngse.2015.12.001.

Khan, A.R., Richardson, J.F., 1987. The Resistance to motion of a solid sphere in a fluid. Chem. Eng. Commun. 62, 135–150. https://doi.org/10.1080/00986448708912056.

Levenspiel, O., Haider, A., 1989. Drag coefficient and terminal velocity of spherical and nonspherical particles. Powder Technol. 58, 63–70.

Machač, I., Ulbrichová, I., Elson, T.P., Cheesman, D.J., 1995. Fall of spherical particles through non-Newtonian suspensions. Chem. Eng. Sci. 50, 3323–3327. https://doi.org/10.1016/0009-2509(95)00168-5.

Morsi, S.A., Alexander, A.J., 1972. An investigation of particle trajectories in two-phase flow systems. J. Fluid Mech. 55, 193–208. https://doi.org/10.1017/S0022112072001806.

Okesanya, T., Abdukarimov, A., Kuru, E., 2020. Generalized models for predicting the drag coefficient and settling velocity of rigid spheres in viscoelastic and viscoinelastic power-law fluids. J. Petrol. Sci. Eng. 191, 107077. https://doi.org/10.1016/j.petrol.2020.107077.

Okesanya, T., Kuru, E., 2019. A new generalized model for predicting particle settling velocity in viscoplastic fluids. SPE Annu. Tech. Conf. Exhib. https://doi.org/10.2118/196104-MS.

Ramírez, C.A., 2017. Summary of frictional drag coefficient relationships for spheres: evolving solution strategies applied to an old problem. Chem. Eng. Sci. 168, 339–343. https://doi.org/10.1016/j.ces.2017.04.037.

Sayindla, S., Lund, B., Ytrehus, J.D., Saasen, A., 2017. Hole-cleaning performance comparison of oil-based and water-based drilling fluids. J. Petrol. Sci. Eng. 159, 49–57. https://doi.org/10.1016/j.petrol.2017.08.069.

Schiller, L., Neumann, A., 1933. A Drag Coefficient Correlation, vol. 77. VDI-Zeits, pp. 318–320.

Shahi, S., Kuru, E., 2015. An experimental investigation of settling velocity of natural sands in water using Particle Image Shadowgraph. Powder Technol. 281, 184–192. https://doi.org/10.1016/j.powtec.2015.04.065.

Stokes, G.G., 1851. On the effect of the internal friction of fluids on the motion of pendulums. Trans. Cambridge Philos. Soc. 9 (Part II), 8–106.

Sun, X., Zhang, K., Chen, Y., Li, W., Qu, J., 2020. Study on the settling velocity of drilling cuttings in the power law fluid. Powder Technol. 362, 278–287. https://doi.org/10.1016/j.powtec.2019.11.025.
Wang, Y., Zhou, L., Wu, Y., Yang, Q., 2018. New simple correlation formula for the drag coefficient of calcareous sand particles of highly irregular shape. Powder Technol. 326, 379–392. https://doi.org/10.1016/j.powtec.2017.12.004.
Xu, Z., Song, X., Li, G., Pang, Z., Zhu, Z., 2019. Settling behavior of non-spherical particles in power-law fluids: experimental study and model development. Particuology 46, 30–39. https://doi.org/10.1016/j.partic.2018.07.006.